



# Asymptotic preserving schemes for the Wigner–Poisson–BGK equations in the diffusion limit

Nicolas Crouseilles<sup>a,\*</sup>, Giovanni Manfredi<sup>b</sup>

<sup>a</sup> Inria Rennes-Bretagne Atlantique, IPSO Project & IRMAR (UMR 6625) Université de Rennes 1, France

<sup>b</sup> Institut de Physique et Chimie des Matériaux de Strasbourg, CNRS and Université de Strasbourg, UMR 7504, F-67034 Strasbourg, France



## ARTICLE INFO

### Article history:

Received 4 November 2012

Received in revised form

30 May 2013

Accepted 2 June 2013

Available online 11 June 2013

### Keywords:

Wigner equation

Diffusion limit

Asymptotic preserving schemes

## ABSTRACT

This work focuses on the numerical simulation of the Wigner–Poisson–BGK equation in the diffusion asymptotics. Our strategy is based on a “micro–macro” decomposition, which leads to a system of equations that couple the macroscopic evolution (diffusion) to a microscopic kinetic contribution for the fluctuations. A semi-implicit discretization provides a numerical scheme which is stable with respect to the small parameter  $\varepsilon$  (mean free path) and which possesses the following properties: (i) it enjoys the asymptotic preserving property in the diffusive limit; (ii) it recovers a standard discretization of the Wigner–Poisson equation in the collisionless regime. Numerical experiments confirm the good behavior of the numerical scheme in both regimes. The case of a spatially dependent  $\varepsilon(x)$  is also investigated.

© 2013 Elsevier B.V. All rights reserved.

## 1. Introduction

The ongoing miniaturization of microelectronics devices makes classical transport models (e.g., the drift-diffusion equation) unable to capture the main features of a variety of systems – such as semiconductor quantum dots and resonant tunneling diodes – where quantum mechanical effects are expected to play a central role. This fact motivates the development of quantum transport models for charged particle systems.

The Wigner representation [1,2] is a useful tool to express quantum mechanics in a phase space formalism. In this representation, a quantum state is described by a Wigner function (i.e., a function of the phase space variables), whose temporal evolution obeys an integro-differential equation (Wigner equation) that is similar to the classical Liouville equation. The Wigner function cannot be regarded as a true probability density in the phase space, as it may take negative values. Nevertheless, it can be used to compute averages just like in classical statistical mechanics.

The Wigner equation can be coupled to the Poisson equation for the electrostatic potential to obtain a suitable model to describe the quantum dynamics of electrons [3,4]. Such self-consistent Wigner–Poisson equations have been extensively used to study quantum transport in semiconductors and metallic nanostructures, such as nanoparticles and thin films [5,6]. A large literature

on the numerical analysis of Wigner–Poisson schemes also exists—see for instance Refs. [7–10].

In semiconductor devices, the electron motion is coupled to the ion lattice vibrations (phonons) which act as a thermal bath driving the electron population toward classical equilibrium on a timescale  $\tau$  [6]. Therefore, in order to deal with a wide range of physical regimes, it is important to construct a numerical model that is stable and accurate both in the fully quantum regime ( $\tau$  large compared to some typical timescale) and in the classical collision-dominated regime ( $\tau$  small).

In the present context, the classical limit model is the drift-diffusion (DD) equation, corresponding to the limit  $\tau \approx \varepsilon \rightarrow 0$  in the scaled Wigner equation (2.1). Our purpose is to design an efficient asymptotic-preserving (AP) scheme for the diffusion asymptotics of the Wigner equation. The term “asymptotic preserving” has been introduced in [11] for numerical schemes that are stable with respect to a small parameter  $\varepsilon$  and degenerate into a consistent numerical scheme for the limit model when  $\varepsilon \rightarrow 0$ . We can also mention the search for macroscopic models containing quantum informations [12–17].

The diffusion limit has already been studied for the radiative transfer equation or the collisional Vlasov equation—we refer the reader to Refs. [18–26] for further details. Other asymptotic limits, such as the fluid limit or the high field limit, have been investigated in Refs. [27–30].

In this work, we study the diffusion limit of the Wigner equation using the so-called “micro–macro” decomposition [27,31,32,29]. This strategy seems to be a robust and systematic way to design AP schemes. The main idea is to develop a micro–macro model

\* Corresponding author. Tel.: +33 2 23 23 58 83.

E-mail address: [nicolas.crouseilles@inria.fr](mailto:nicolas.crouseilles@inria.fr) (N. Crouseilles).

(equivalent to the original Wigner equation) which couples the macroscopic part of the evolution to a microscopic part. A suitable semi-implicit discretization then ensures that the corresponding numerical scheme satisfies the asymptotic-preserving property. However, in the collisionless limit ( $\varepsilon \rightarrow \infty$ ), such a scheme displays a modified time discretization of the original Wigner–Poisson model, which may affect the long-time behavior of the solution. Hence, we introduce a slight improvement that ensures a standard time discretization of the Wigner–Poisson equation in the collisionless limit without affecting the asymptotic-preserving character of the numerical scheme. Note that in [33], an asymptotic preserving scheme has been obtained by separating odd and even part of the unknown.

We shall restrict our analysis to one-dimensional (1D) problems and consider the Wigner distribution function  $f(t, x, v)$ , which depends on time  $t \geq 0$ , space  $x \in [0, L]$  and velocity  $v \in \mathbb{R}$ . Denoting by  $\phi(t, x)$  the self-consistent electric potential ( $E = -\partial_x \phi$  is the electric field), the collisional Wigner equation reads as (with  $e$  and  $m$  representing the electron charge and mass, respectively)

$$\frac{\partial f}{\partial t} + v \partial_x f - \frac{e}{m} T_{h/m}[\phi] f = \frac{1}{\tau} Q(f), \quad (1.1)$$

where  $\tau$  is a relaxation time and

$$\begin{aligned} (T_{h/m}[\phi] f)(t, x, v) \\ = \frac{i}{2\pi} \int_{\mathbb{R}_\xi} \int_{\mathbb{R}_{v'}} \frac{\phi(t, x + \frac{h}{2m} \xi) - \phi(t, x - \frac{h}{2m} \xi)}{h/m} \\ \times f(t, x, v') \exp[-i(v - v') \xi] dv' d\xi, \end{aligned}$$

with  $\hbar$  the Planck constant. The self-consistent potential obeys the Poisson equation

$$\partial_x^2 \phi(t, x) = -e[\rho(t, x) - n_i(x)], \quad (1.2)$$

where  $\rho(t, x) = \int_{\mathbb{R}} f(t, x, v) dv$  and  $n_i$  is a given ion density. The collision operator  $Q(f)$  is the Bhatnagar–Gross–Krook (BGK) collision operator

$$Q(f)(t, x, v) = \rho(t, x) M_\Theta(v) - f(t, x, v),$$

$$\text{with } M_\Theta(v) = \frac{1}{\sqrt{2\pi\Theta}} \exp\left(-\frac{v^2}{2\Theta}\right), \quad (1.3)$$

with  $\Theta = k_B T / m$ ,  $k_B$  being the Boltzmann constant and  $T$  a given temperature.

We consider a spatially periodic plasma with period  $L$ . The distribution function  $f$  satisfies the following boundary conditions:

$$f(t, 0, v) = f(t, L, v), \quad \forall v \in \mathbb{R}, t \geq 0. \quad (1.4)$$

In order to obtain a well-posed problem, a zero-mean condition has to be imposed on the electric field:

$$\int_0^L E(t, x) dx = 0, \quad \forall t \geq 0. \quad (1.5)$$

Finally, an initial condition should be specified

$$f(0, x, v) = f_0(x, v), \quad \forall x \in [0, L], v \in \mathbb{R}. \quad (1.6)$$

The rest of the paper is organized as follows. In Section 2, the diffusive scaling and the corresponding asymptotics are presented in the Wigner–BGK case. In Section 3, a linear stability analysis is performed and the relevant growth rate is computed. In Section 4, we present the asymptotic-preserving numerical scheme for the Wigner–BGK equation in the diffusive scaling. The results of several numerical tests are shown in Section 5, and conclusions are finally drawn in Section 6.

## 2. Diffusion regime for Wigner–BGK

In this section, we detail the diffusion scaling for (1.1) and the corresponding asymptotic model (we refer the reader to [34] for more details).

### 2.1. Diffusion scaling

We normalize space to a characteristic macroscopic length  $\ell$ , velocity to the thermal speed  $\sqrt{\Theta}$ , and time to  $\ell/U_0$ , where  $U_0$  is a typical drift velocity. The electric potential is normalized to  $m\Theta/e$  and the electron density to the average density  $\rho_0$ . We also assume that the ion density profile is uniform, i.e.,  $n_i(x) = \rho_0$ .

With these normalizations, the Wigner–BGK equation becomes

$$\eta \partial_t f + v \partial_x f - T_{v h_0}[\phi] f = \frac{1}{v} (\rho M_\Theta - f),$$

and the Poisson equation can be written as

$$\partial_x^2 \phi = -\gamma(\rho - 1),$$

where  $\eta = U_0/\sqrt{\Theta}$ ,  $v = \sqrt{\Theta}\tau/\ell$ , and  $\gamma = \rho_0 e^2 \ell^2 / (m\Theta \epsilon_0) = \omega_p^2 \ell^2 / \Theta = \ell^2 / \lambda_D^2$ , where  $\lambda_D$  is the Debye length. In the forthcoming simulations, we will always take  $\gamma = 1$ .

In the diffusion regime, we assume that  $\eta = v = \varepsilon \ll 1$ , which means that the drift velocity  $U_0 \sim \varepsilon$  is small compared to the thermal velocity  $\sqrt{\Theta} \sim 1$ , which in turn is small compared to the relaxation velocity  $\ell/\tau \sim \varepsilon^{-1}$ . The relevant ordering can thus be written as

$$U_0 \ll \sqrt{\Theta} \ll \frac{\ell}{\tau}.$$

With the above scaling, the Wigner equation becomes

$$\varepsilon \partial_t f + v \partial_x f - T_{\varepsilon h_0}[\phi] f = \frac{1}{\varepsilon} (\rho M_\Theta - f), \quad (2.1)$$

where the normalized Planck constant  $h_0$  is defined as

$$h_0 = \frac{\hbar}{m\Theta\tau},$$

and

$$\begin{aligned} T_{\varepsilon h_0}[\phi] f = \frac{i}{2\pi} \int_{\mathbb{R}_\xi} \int_{\mathbb{R}_{v'}} \frac{\phi(t, x + \frac{\varepsilon h_0}{2} \xi) - \phi(t, x - \frac{\varepsilon h_0}{2} \xi)}{\varepsilon h_0} \\ \times f(t, x, v') \exp[-i(v - v') \xi] dv' d\xi. \end{aligned}$$

### 2.2. Derivation of the asymptotic drift-diffusion model

To derive the DD model from Eq. (2.1) in the asymptotic limit  $\varepsilon \rightarrow 0$ , the usual procedure is to perform a Hilbert expansion of the Wigner function:  $f = f_0 + \varepsilon f_1 + \varepsilon^2 f_2$ . This expansion is injected in (2.1), and the terms of same order are identified. At the lowest order  $\varepsilon^{-2}$ , we obtain

$$f_0(t, x, v) = \rho(t, x) M_\Theta(v), \quad \rho(t, x) = \int f_0(t, x, v) dv.$$

In particular, the first moment of  $f$  is equal to the first moment of  $f_0$ ; as a consequence, the first moment of  $f_1$  and  $f_2$  is equal to zero. Identifying terms of order  $\varepsilon^{-1}$ , we find that  $f_1$  has to satisfy

$$v \partial_x f_0 - \partial_x \phi \partial_v f_0 = -f_1. \quad (2.2)$$

This equation has a solution if and only if the right hand side satisfies the null average condition:

$$\int (v \partial_x f_0 - \partial_x \phi \partial_v f_0) dv = 0.$$

Using the relation  $f_0 = \rho M_\Theta$ , we have  $\int_{\mathbb{R}} v \partial_x f_0 dv = 0$ , and  $\int_{\mathbb{R}} \partial_x \phi \partial_v f_0 dv = 0$ . Hence, the integral of the right hand side of (2.2) is equal to zero and (2.2) has a unique solution  $f_1$  given by

$$f_1 = -v \partial_x f_0 + \partial_x \phi \partial_v f_0. \quad (2.3)$$

Finally, keeping terms of order unity leads to

$$\partial_t f_0 + v \partial_x f_1 - T_{\varepsilon h_0}[\phi] f_1 = Q(f_2) = -f_2.$$

The solvability condition for  $f_2$  implies that

$$\partial_t \rho + \partial_x \left( \int_{\mathbb{R}} v f_1 dv \right) = 0, \quad (2.4)$$

since  $\int T_{\varepsilon h_0}[\phi] f_1 dv = 0$ . Using (2.3), we get

$$\begin{aligned} \int_{\mathbb{R}} v f_1 dv &= -\partial_x \int_{\mathbb{R}} v^2 f_0 dv + \int_{\mathbb{R}} v \partial_x \phi \partial_v f_0 dv \\ &= -\partial_x(\rho \Theta) - \rho \partial_x \phi, \end{aligned}$$

so that (2.4) becomes the so-called DD equation

$$\partial_t \rho - \partial_x [\rho \partial_x \phi + \partial_x(\rho \Theta)] = 0. \quad (2.5)$$

### 2.3. Derivation of the micro-macro model and the asymptotic limit

This section is devoted to the derivation of the micro-macro model starting from the Wigner–BGK equation (see [27,29,32,31]).

*Derivation of the micro-macro model*

Let us suppose that  $f$  satisfies the following decomposition (we assume  $\Theta = 1$  for simplicity)

$$f = \rho M + g, \quad \text{with } M(v) = \frac{1}{\sqrt{2\pi}} \exp\left(-\frac{v^2}{2}\right), \quad \rho = \int f dv.$$

We introduce the transport operator  $\mathcal{T}f = v \partial_x f - T_{\varepsilon h_0}[\phi] f$  of the Wigner equation (1.1), which leads to

$$\partial_t(\rho M) + \partial_t g + \frac{1}{\varepsilon} \mathcal{T}(\rho M) + \frac{1}{\varepsilon} \mathcal{T}g = -\frac{1}{\varepsilon^2} g. \quad (2.6)$$

We define  $\Pi$  as the orthogonal projection in  $L^2(M^{-1}dv)$ , endowed with the weighted scalar product  $(\varphi, \psi)_M = \langle \varphi \psi M^{-1} \rangle = \int (\varphi \psi / M) dv$ , onto the kernel of the collision operator

$$\mathcal{N}(Q) = \left\{ f = \rho M \text{ where } \rho = \int f dv \right\}.$$

For any function  $\varphi$  depending on  $v$ , the explicit orthogonal projection onto the kernel is given by

$$\Pi(\varphi) = \int \varphi dv M. \quad (2.7)$$

In this case, the projection is nothing but an integration in  $v$  multiplied by the Maxwellian function. But this approach is general and can be adapted to different cases (see [27,29,32,31,35]).

The micro-macro model is obtained by applying  $\Pi$  and  $(I - \Pi)$  to (2.6). Applying  $\Pi$  to (2.6) provides an equation for  $\rho$ , whereas applying  $(I - \Pi)$  gives an equation for  $g$ . The micro-macro model of unknown  $(\rho, g, \phi)$  can then be written

$$\begin{cases} \partial_t g + \frac{1}{\varepsilon} (I - \Pi) \mathcal{T}g \\ \quad = \frac{1}{\varepsilon^2} [-g - \varepsilon (I - \Pi) \mathcal{T}(\rho M)], & \text{“micro”} \\ \partial_t \rho + \frac{1}{\varepsilon} \partial_x \int v g dv = 0, & \text{“macro”} \\ \partial_x^2 \phi = -(\rho - 1), & \text{“Poisson”} \end{cases} \quad (2.8)$$

where  $\Pi$  is defined in (2.7),  $\mathcal{T}g = v \partial_x g - T_{\varepsilon h_0}[\phi] g$  and  $M(v) = (1/\sqrt{2\pi}) \exp(-v^2/2)$ . This micro-macro model is a good candidate to construct an asymptotic preserving scheme, as was done in Refs. [31,29], since the asymptotic model is already almost contained in the “macro” part of the above formulation.

**Proposition 2.1.** (i) If  $(f, \phi)$  is a solution of (1.1)–(1.2)–(1.3) with the initial data (1.6), then  $(\rho, g, \phi) = (\int f dv, f - \rho M, \phi)$  is a solution of (2.8) with the associated initial data

$$\begin{aligned} \rho(t=0) &= \int f(t=0) dv, \\ g(t=0) &= f(t=0) - \rho(t=0)M, \quad \text{and} \\ \partial_x^2 \phi(t=0) &= -(\rho(t=0) - 1). \end{aligned} \quad (2.9)$$

(ii) Conversely, if  $(\rho, g, \phi)$  is a solution of (2.8) with initial data (2.9), then  $\int g dv = 0$  and  $f = \rho M + g$  is a solution of (1.1)–(1.2)–(1.3).

*Chapman–Enskog expansion*

In this paragraph, we want to verify formally that the asymptotic limit of (2.8) is indeed the DD model (2.5) derived previously. Multiplying the first equation of (2.8) by  $\varepsilon^2$ , we deduce that  $g = \mathcal{O}(\varepsilon)$  so that we can write from the first equation of (2.8),

$$\begin{aligned} g &= -\varepsilon(I - \Pi) \mathcal{T}(\rho M) + \mathcal{O}(\varepsilon^2) \\ &= -\varepsilon(I - \Pi)(vM \partial_x \rho - T_{\varepsilon h_0}[\phi](\rho M)) + \mathcal{O}(\varepsilon^2), \\ &= -\varepsilon(I - \Pi)(vM \partial_x \rho - \partial_x \phi \partial_v(\rho M)) + \mathcal{O}(\varepsilon^2) \\ &= -\varepsilon(vM \partial_x \rho - \partial_x \phi \partial_v(\rho M)) + \mathcal{O}(\varepsilon^2) \\ &= -\varepsilon(vM \partial_x \rho + v \rho M \partial_x \phi) + \mathcal{O}(\varepsilon^2). \end{aligned}$$

If we now inject the above expression into the second equation of (2.8), we obtain

$$\partial_t \rho - \partial_x \left[ \int v^2 M dv \partial_x \rho + \rho \partial_x \phi \right] = \mathcal{O}(\varepsilon^2)$$

or, when  $\varepsilon$  goes to zero,

$$\partial_t \rho - \partial_x [\partial_x \rho + \rho \partial_x \phi] = 0, \quad (2.10)$$

which is exactly the drift-diffusion model (2.5).

These basic computations will be mimicked at the discrete level.

### 3. Linear stability analysis

In this section, we study the linear response of the Wigner–BGK equations in order to validate the collisionless limit (i.e.,  $\varepsilon \rightarrow \infty$  in (2.1)) in the numerical simulations. Note that the forthcoming calculations are performed only at a formal level, with the aim of deriving a damping (or instability) rate that can be compared to the numerical results of Section 5. Regularity conditions on  $f$  will not be addressed.

In order to investigate the linear response of the Wigner–Poisson equations, we expand the distribution function and the potential around the equilibrium solution  $f = f_0(v)$ ,  $\phi = 0$ :

$$f(t, x, v) = f_0(v) + f_1(t, x, v), \quad \phi(t, x) = \phi_1(t, x), \quad (3.1)$$

and then neglect second order terms. Further, we assume that the perturbed quantities can be expanded in a Fourier series both in space and in time, i.e.:

$$\begin{aligned} f_1(x, v, t) &= \tilde{f}_1(v) \exp(-i\omega t + ikx), \\ \phi_1(x, t) &= \tilde{\phi}_1 \exp(-i\omega t + ikx), \end{aligned}$$

where  $\omega$  and  $k$  are the frequency and the wave number of the perturbation, respectively.

We first apply this approach to the Wigner–Poisson equations without the BGK term, which disappears in the limit  $\varepsilon \rightarrow \infty$ . In this case, the relevant dispersion relation can be written in terms of the Lindhardt “dielectric constant” [36]

$$\begin{aligned} D(\Omega, k) &\equiv 1 + \frac{1}{Hk^2} \\ &\times \int_{-\infty}^{+\infty} \frac{f_0(v + Hk/2) - f_0(v - Hk/2)}{\Omega - kv} dv = 0, \end{aligned} \quad (3.2)$$

where we have defined  $\Omega = \omega \varepsilon$  and  $H = h_0 \varepsilon$ .

Expanding in a Taylor series the difference term in the integral in Eq. (3.2), we obtain

$$D(\Omega, k) \approx 1 + \frac{1}{k} \int \frac{f'_0(v)}{\Omega - kv} dv + \frac{H^2 k}{24} \int \frac{f'''_0(v)}{\Omega - kv} dv + \dots \quad (3.3)$$

where the apex denotes derivation with respect to  $v$ . Notice that the first two terms are identical to the dispersion relation for the Vlasov–Poisson equations, whereas the last term is a quantum correction.

We further assume that the wave number of the perturbation is small, i.e.,  $kv \ll \Omega$ , and use this fact to write the following expansion:

$$\frac{1}{\Omega - kv} \approx \frac{1}{\Omega} + \frac{kv}{\Omega^2} + \frac{k^2 v^2}{\Omega^3} + \frac{k^3 v^3}{\Omega^4} + \dots$$

If the equilibrium distribution  $f_0(v)$  is an even function of  $v$ , the dielectric constant can then be expressed in the following way:

$$D(\Omega, k) \approx 1 - \frac{1}{\Omega^2} - \frac{3k^2 \langle v^2 \rangle}{\Omega^4} - \frac{H^2 k^4}{4\Omega^4}, \quad (3.4)$$

where  $\langle v^2 \rangle := \int v^2 f_0(v) dv$ , or, equivalently to the relevant order

$$D(\Omega, k) \approx 1 - \left\{ \Omega^2 - 3k^2 \theta - \frac{H^2 k^4}{4} \right\}^{-1}, \quad (3.5)$$

where we have used the fact that, for a Maxwellian distribution  $f_0(v) = M_\theta(v)$ , we have  $\langle v^2 \rangle = \theta$ . Note that another equilibrium can be considered; see [37] for the Lorentzian equilibrium case.

Now, for an equilibrium distribution shifted by a constant velocity  $\pm V$ , the above dispersion relation becomes

$$D_\pm(\Omega, k) = 1 - \left\{ (\Omega \pm kV)^2 - 3k^2 \theta - \frac{H^2 k^4}{4} \right\}^{-1}. \quad (3.6)$$

In the forthcoming sections, we will be interested in two-stream distributions composed of two Maxwellians traveling with velocities  $\pm V$ . In that case, the dielectric constant can be written as

$$D(\Omega, k) = \frac{D_+(\Omega, k) + D_-(\Omega, k)}{2}. \quad (3.7)$$

Setting  $D(k, \omega) = 0$ , we obtain the dispersion relation for the two-stream plasma

$$\begin{aligned} \Omega^4 - \left( 1 + 2k^2(V^2 + 3\theta) + \frac{H^2 k^4}{2} \right) \Omega^2 \\ - k^2 \left( V^2 - 3\theta - \frac{H^2 k^2}{4} \right) \\ \times \left( 1 - (V^2 - 3\theta)k^2 + \frac{H^2 k^4}{4} \right) = 0. \end{aligned} \quad (3.8)$$

Solving for  $\Omega^2$ , one obtains

$$\begin{aligned} \Omega^2 = \frac{1}{2} + k^2 \left( V^2 + 3\theta + \frac{H^2 k^2}{4} \right) \\ \pm \frac{1}{2} \left[ 1 + 8k^2 \left( V^2 + 6k^2 \theta + \frac{H^2 k^4}{2} \right) \right]^{1/2}. \end{aligned} \quad (3.9)$$

Instability occurs when  $\Omega^2 < 0$ , and the instability rate is simply given by  $\text{Im}(\Omega)/\varepsilon$  (see Fig. 1).

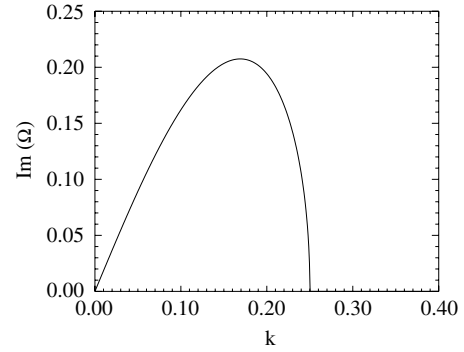


Fig. 1. Plot of the instability rate for a two-stream distribution,  $h_0 = 0.01$ ,  $\varepsilon = 1000$ ,  $V = 2$ ,  $\theta = 0.2$ .

#### 4. Numerical approximation

In the following, we introduce a formal discrete finite difference operator for the spatial derivative  $D_x$  such that  $(D_x f)$  is an approximation of  $\partial_x f$ . Hence we shall reuse the previous continuous notation  $\mathcal{T}f$  in this discrete framework  $\mathcal{T}f = v D_x f - T_{\varepsilon h_0}[\phi^n]f$  (the electric potential is evaluated at time  $t^n$ ).

First, we focus on the time discretization without specifying the spatial discretization ( $D_x$  is used for all spatial derivatives). Then, a detailed full discretization is proposed.

##### 4.1. Time discretizations

###### Semi-implicit time discretization

Following [31,29], the main idea is to treat the stiffest terms in an implicit way. In the micro equation, the stiffest term is  $g/\varepsilon^2$ , whereas in the macro equation the flux  $\int v g dv$  should also be treated implicitly. We then get the following semi-discretization in time for (2.8):

$$\begin{cases} \frac{g^{n+1} - g^n}{\Delta t} + \frac{1}{\varepsilon} (I - \Pi) \mathcal{T} g^n \\ = \frac{1}{\varepsilon^2} [-g^{n+1} - \varepsilon (I - \Pi) \mathcal{T}(\rho^n M)], \\ \frac{\rho^{n+1} - \rho^n}{\Delta t} + \frac{1}{\varepsilon} D_x \int v g^{n+1} dv = 0, \\ -\partial_x^2 \phi^n = \rho^n - 1. \end{cases} \quad (4.1)$$

The first equation can be rewritten as

$$g^{n+1} = \left( 1 + \frac{\varepsilon^2}{\Delta t} \right)^{-1} \left( \frac{\varepsilon^2}{\Delta t} g^n - \varepsilon (I - \Pi) \mathcal{T}(\rho^n M + g^n) \right). \quad (4.2)$$

Once  $g^{n+1}$  has been computed, the macro equation on  $\rho$  can be advanced to get  $\rho^{n+1}$  and the electric potential can be solved to obtain  $\phi^{n+1}$ . This numerical scheme has been proved to be stable independently of  $\varepsilon$ , at least in the linear case (radiative transfer equation) in [31,38].

###### AP property

Let us verify that the previous numerical scheme provides a consistent scheme for (2.5) when  $\varepsilon$  goes to zero. When  $\varepsilon \ll 1$ , we have from the micro equation that  $g^{n+1} = \mathcal{O}(\varepsilon)$ . Then, in this regime, we have from (4.2)

$$\begin{aligned} g^{n+1} &= -\varepsilon (I - \Pi) \mathcal{T}(\rho^n M) + \mathcal{O}(\varepsilon^2), \\ &= -\varepsilon \mathcal{T}(\rho^n M) + \mathcal{O}(\varepsilon^2), \\ &= -\varepsilon (v M D_x \rho^n - T_{\varepsilon h_0}[\phi^n](\rho^n M)) + \mathcal{O}(\varepsilon^2), \\ &= -\varepsilon (v M D_x \rho^n - D_x \phi^n \partial_v(\rho^n M)) + \mathcal{O}(\varepsilon^2), \\ &= -\varepsilon (v M D_x \rho^n + v \rho^n M D_x \phi^n) + \mathcal{O}(\varepsilon^2), \end{aligned}$$

which, injected into the macro equation, leads to

$$\frac{\rho^{n+1} - \rho^n}{\Delta t} - D_x \left( \int v^2 M dv D_x \rho^n + \int v^2 M dv \rho^n D_x \phi^n \right) = 0.$$

Using  $\int v^2 M dv = 1$ , the above equation can be rewritten as

$$\frac{\rho^{n+1} - \rho^n}{\Delta t} - D_x (D_x \rho^n + \rho^n D_x \phi^n) = 0, \quad (4.3)$$

which is an explicit time discretization of the limit model (2.5). Let us also mention that an implicit discretization of the diffusion term  $\partial_x^2 \rho$  can be derived using the methods described in Refs. [32,29]. This numerical scheme is detailed at the end of the present section.

#### Mixed scheme

Here, we want to design a numerical scheme which, in the limit  $\varepsilon \rightarrow +\infty$ , recovers an explicit numerical scheme for the Wigner–Poisson equation

$$f^{n+1} = f^n - \frac{\Delta t}{\varepsilon} \mathcal{T} f^n + \mathcal{O} \left( \frac{1}{\varepsilon^2} \right), \quad (4.4)$$

which was not the case for the above time discretization. Indeed, adding together the first two equations of (4.1) leads to

$$f^{n+1} = f^n - \frac{\Delta t}{\varepsilon} \mathcal{T} f^n - \frac{\Delta t}{\varepsilon} \Pi (v D_x (g^{n+1} - g^n)) + \mathcal{O} \left( \frac{1}{\varepsilon^2} \right),$$

which involves an additional term of order  $\mathcal{O}(\Delta t^2)$  that can pollute the long-time behavior of the numerical solution.

On the other hand, an explicit (but not stable) discretization of the macro equation gives

$$\rho^{n+1} = \rho^n - \frac{\Delta t}{\varepsilon} \int \mathcal{T} f^n dv, \quad (4.5)$$

where  $f^n = \rho^n M + g^n$ . Multiplying Eq. (4.5) by  $M$  and adding to the first of equations (4.1) for  $g$  yields

$$f^{n+1} = f^n - \frac{\Delta t}{\varepsilon} \mathcal{T} f^n + \mathcal{O} \left( \frac{1}{\varepsilon^2} \right).$$

If the transport dominates over the dissipation phenomena (which occurs when  $\varepsilon \rightarrow +\infty$ ), then one would like to recover this discretization of the initial kinetic equation.

One way to derive a numerical scheme that is well behaved both when  $\varepsilon \rightarrow 0$  and when  $\varepsilon \rightarrow \infty$  is to combine the flux in (4.5) with the flux  $\Pi(v D_x g^{n+1})$ . To that purpose, we choose a linear combination of these two fluxes

$$\begin{aligned} \rho^{n+1} = & \rho^n - \beta \frac{\Delta t}{\varepsilon} \int \mathcal{T} f^n dv \\ & - (1 - \beta) \frac{\Delta t}{\varepsilon} D_x \int (v g^{n+1}) dv, \end{aligned} \quad (4.6)$$

where we require  $\beta$  to satisfy the following properties:

- $\beta \in [0, 1]$ , for the consistency;
- $\beta = \mathcal{O}(\varepsilon^2)$  when  $\varepsilon \rightarrow 0$ , to preserve the AP property;
- $\lim_{\varepsilon \rightarrow \infty} \beta = 1$  to ensure the correct collisionless limit when  $\varepsilon \rightarrow +\infty$ .

One good choice appears to be  $\beta = \varepsilon^2/(1 + \varepsilon^2)$ .

Hence, we still keep the consistency with respect to the initial model for a fixed  $\varepsilon > 0$  since we have used a linear combination of two consistent fluxes with  $\beta \in [0, 1]$ . Moreover, when  $\varepsilon \rightarrow 0$ , we have  $\beta/\varepsilon \rightarrow 0$  so that we recover the previous stable discretization

$$\rho^{n+1} = \rho^n - \frac{\Delta t}{\varepsilon} D_x \int (v g^{n+1}) dv + \mathcal{O}(\varepsilon),$$

which is consistent with the limit drift-diffusion model (see above). On the other hand, when  $\varepsilon \rightarrow +\infty$ , we have  $\beta \rightarrow 1$  so that we recover

$$\rho^{n+1} = \rho^n - \frac{\Delta t}{\varepsilon} \int \mathcal{T} f^n dv + \mathcal{O} \left( \frac{1}{\varepsilon^2} \right),$$

which, added to the equation for  $g$  (i.e., the first equation of (4.1)), leads to the explicit discretization (4.4) of the initial Wigner–Poisson equation.

#### Implicit diffusion

Following Refs. [32,29], it is possible to obtain, in the diffusion limit, a numerical scheme in which the diffusion term is implicit. This is of great interest since the restrictive condition  $\Delta t = \mathcal{O}(\Delta x^2)$  can be avoided when one deals with small values of  $\varepsilon$ . We now provide some details on this strategy in the context of the Wigner–BGK equation.

First, we rewrite  $g^{n+1}$  from (4.2)

$$\begin{aligned} g^{n+1} &= \frac{\varepsilon^2}{\Delta t + \varepsilon^2} g^n - \frac{\varepsilon \Delta t}{\Delta t + \varepsilon^2} (I - \Pi) \mathcal{T} (\rho^n M + g^n) \\ &= \frac{\varepsilon^2}{\Delta t + \varepsilon^2} g^n - \frac{\varepsilon \Delta t}{\Delta t + \varepsilon^2} [v M D_x \rho^n + (I - \Pi) v D_x g^n \\ &\quad - T_{\varepsilon h_0} [\phi^n] (\rho^n M + g^n)] \\ &= h^n - \frac{\varepsilon \Delta t}{\Delta t + \varepsilon^2} v M D_x \rho^n, \end{aligned}$$

where  $h^n$  is defined as  $h^n = g^{n+1} + [\varepsilon \Delta t / (\Delta t + \varepsilon^2)] v M D_x \rho^n$ . Injecting this expression of  $g^{n+1}$  into (4.6), we get

$$\begin{aligned} \rho^{n+1} &= \rho^n - \beta \frac{\Delta t}{\varepsilon} \int \mathcal{T} f^n dv - (1 - \beta) \frac{\Delta t}{\varepsilon} D_x \int (v g^{n+1}) dv \\ &= \rho^n - \beta \frac{\Delta t}{\varepsilon} \int \mathcal{T} f^n dv \\ &\quad - (1 - \beta) \frac{\Delta t}{\varepsilon} D_x \int v h^n dv + (1 - \beta) \frac{\Delta t^2}{\Delta t + \varepsilon^2} D_x \\ &\quad \times \int v^2 M dv D_x \rho^n. \end{aligned}$$

The last term can be considered implicit so that the macro equation becomes

$$\begin{aligned} \rho^{n+1} &= \rho^n - \beta \frac{\Delta t}{\varepsilon} \int \mathcal{T} f^n dv - (1 - \beta) \frac{\Delta t}{\varepsilon} D_x \\ &\quad \times \int v h^n dv + (1 - \beta) \frac{\Delta t^2}{\Delta t + \varepsilon^2} D_x \\ &\quad \times \int v^2 M dv D_x \rho^{n+1}, \end{aligned} \quad (4.7)$$

coupled with the micro equation

$$g^{n+1} = h^n - \frac{\varepsilon \Delta t}{\Delta t + \varepsilon^2} v M D_x \rho^n, \quad (4.8)$$

with  $h^n$  given by

$$\begin{aligned} h^n &= \frac{\varepsilon^2}{\Delta t + \varepsilon^2} g^n - \frac{\varepsilon \Delta t}{\Delta t + \varepsilon^2} [(I - \Pi) v D_x g^n - T_{\varepsilon h_0} \\ &\quad \times [\phi^n] (\rho^n M + g^n)]. \end{aligned} \quad (4.9)$$



## 4.2. Full discretization

Starting with the numerical method proposed in [39], we derive a numerical scheme for (2.8), in particular for the numerical resolution of  $T_{\varepsilon h_0}[\phi]$ .

Let us denote  $x_i = i\Delta x$ ,  $i = -1, \dots, N_x$  and  $v_k = v_{\min} + k\Delta v$ ,  $k = 0, \dots, N_v - 1$  where  $\Delta x = L/N_x$  and  $\Delta v = (v_{\max} - v_{\min})/N_v$  (with  $v_{\max} = -v_{\min}$ ) are the uniform phase space discretizations. Hence we denote by  $g_{i,k}^n$  an approximation of  $g(t^n, x_i, v_k)$  and  $M_k = M(v_k)$ . On the other hand, the macro part of (2.8) is approximated at  $x_i = i\Delta x$ ,  $i = 0, \dots, N_x$  so that we use the notations  $\rho_i^n \approx \rho(t^n, x_i)$ . The electric potential is evaluated at  $x_i$  by  $\phi_i(t^n)$  and we can reconstruct the total distribution function  $f_{i,k}^n = \rho_i^n M_k + g_{i,k}^n$ .

Recalling that  $\mathcal{T} = v\partial_x - T_{\varepsilon h_0}[\phi^n]$ , we use a finite volume scheme for the transport in the spatial variable to get the following approximation for  $(\mathcal{T}f)(t^n, x_i, v_j)$ :

$$(\mathcal{T}f)_{i,k} = v_k^+ \frac{f_{i,k}^n - f_{i-1,k}^n}{\Delta x} + v_k^- \frac{f_{i+1,k}^n - f_{i,k}^n}{\Delta x} - T_{\varepsilon h_0}[\phi^n]_{i,k}^n,$$

so that the numerical scheme for (4.2) reads as

$$g_{i,k}^{n+1} \left( 1 + \frac{\varepsilon^2}{\Delta t} \right) = \frac{\varepsilon^2}{\Delta t} g_{i,k}^n - \varepsilon(I - \Pi)(\mathcal{T}f)_{i,k}^n. \quad (4.10)$$

Here the projection  $\Pi f$  is approximated by the following discrete operator  $(\Pi f)_{i,k} \approx (\sum_k f_{i,k} \Delta v) M_k$ , whereas the integrals in  $v$  are approximated by a sum on the discrete velocities. Once  $g_{i,k}^{n+1}$  is computed, the time-stepping of the macro equation is

$$\begin{aligned} \rho_i^{n+1} &= \rho_i^n - \beta \frac{\Delta t}{\varepsilon} \left( \sum_k (\mathcal{T}f)_{i,k} \Delta v \right) - (1 - \beta) \frac{\Delta t}{\varepsilon} \\ &\quad \times \sum_k \left( v_k \frac{g_{i+1,k}^{n+1} - g_{i-1,k}^{n+1}}{2\Delta x} \Delta v \right). \end{aligned} \quad (4.11)$$

The Poisson equation can be discretized to get the potential at  $x_i$ :

$$-[\phi_{i+1}^n - 2\phi_i^n + \phi_{i-1}^n] = \Delta x^2 (\rho_i^n - 1). \quad (4.12)$$

Finally, the Wigner term  $T_{\varepsilon h_0}[\phi^n]$  is discretized using the spectral method described in Ref. [39].

The asymptotic property can also be proven in the fully discretized context. Indeed, in the discrete micro equation for  $g$ , we get as  $\varepsilon$  goes to zero

$$\begin{aligned} g_{i,k}^{n+1} &= -\varepsilon(I - \Pi) \left[ v_k^+ \frac{f_{i,k}^n - f_{i-1,k}^n}{\Delta x} \right. \\ &\quad \left. + v_k^- \frac{f_{i+1,k}^n - f_{i,k}^n}{\Delta x} - T_{\varepsilon h_0}[\phi^n]_{i,k}^n \right] + \mathcal{O}(\varepsilon^2), \\ &= -\varepsilon(I - \Pi) \left[ M_k v_k^+ \frac{\rho_i^n - \rho_{i-1}^n}{\Delta x} \right. \\ &\quad \left. + M_k v_k^- \frac{\rho_{i+1}^n - \rho_i^n}{\Delta x} - T_{\varepsilon h_0}[\phi^n]_{i,k}^n \right] + \mathcal{O}(\varepsilon^2), \\ &= -\varepsilon \left[ M_k v_k^+ \frac{\rho_i^n - \rho_{i-1}^n}{\Delta x} + M_k v_k^- \frac{\rho_{i+1}^n - \rho_i^n}{\Delta x} \right. \\ &\quad \left. + \varepsilon \frac{\rho_i^n - \rho_{i-1}^n}{\Delta x} \Pi(M_k v_k^+) + \varepsilon \frac{\rho_{i+1}^n - \rho_i^n}{\Delta x} \right. \\ &\quad \left. \times \Pi(M_k v_k^-) + \varepsilon T_{\varepsilon h_0}[\phi^n]_{i,k}^n + \mathcal{O}(\varepsilon^2) \right], \\ &= -\varepsilon \left[ M_k v_k^+ \frac{\rho_i^n - \rho_{i-1}^n}{\Delta x} + M_k v_k^- \frac{\rho_{i+1}^n - \rho_i^n}{\Delta x} \right] \end{aligned}$$

$$\begin{aligned} &+ \varepsilon \frac{\rho_i^n - \rho_{i-1}^n}{\Delta x} \Pi(M_k |v_k|)/2 - \varepsilon \frac{\rho_{i+1}^n - \rho_i^n}{\Delta x} \\ &\quad \times \Pi(M_k |v_k|)/2 + \varepsilon T_{\varepsilon h_0}[\phi^n]_{i,k}^n + \mathcal{O}(\varepsilon^2), \\ &= -\varepsilon \left[ M_k v_k^+ \frac{\rho_i^n - \rho_{i-1}^n}{\Delta x} + M_k v_k^- \frac{\rho_{i+1}^n - \rho_i^n}{\Delta x} \right] \\ &\quad + \varepsilon \frac{2\rho_i^n - \rho_{i+1}^n - \rho_{i-1}^n}{2\Delta x} \Pi(M_k |v_k|)/2 \\ &\quad + \varepsilon T_{\varepsilon h_0}[\phi^n]_{i,k}^n + \mathcal{O}(\varepsilon^2), \\ &= -\varepsilon M_k v_k \frac{\rho_{i+1}^n - \rho_{i-1}^n}{2\Delta x} + \varepsilon \frac{\rho_{i+1}^n - 2\rho_i^n + \rho_{i-1}^n}{2\Delta x} \\ &\quad \times (I - \Pi)(M_k |v_k|) + \varepsilon T_{\varepsilon h_0}[\phi^n]_{i,k}^n + \mathcal{O}(\varepsilon^2). \end{aligned}$$

But  $(I - \Pi)(M_k |v_k|) = M_k(|v_k| - \sqrt{2/\pi})$ , which is even, so that  $v_k(I - \Pi)(M_k |v_k|)$  is odd and  $\Pi(v_k(I - \Pi)(M_k |v_k|)) = 0$ . Then, injecting  $g_{i,k}^{n+1}$  into (4.11) leads to

$$\begin{aligned} &\frac{\rho_i^{n+1} - \rho_i^n}{\Delta t} \\ &= \Pi(v_k^2 M_k) \frac{\rho_{i+2}^n - 2\rho_i^n + \rho_{i-2}^n}{4\Delta x^2} \\ &\quad - \frac{\Pi(v_k T_{\varepsilon h_0}[\phi^n]_{i+1,k}^n) - \Pi(v_k T_{\varepsilon h_0}[\phi^n]_{i-1,k}^n)}{2\Delta x} + \mathcal{O}(\varepsilon), \\ &= \partial_x [\partial_x \rho^n + \rho^n \partial_x \phi^n]_i + \mathcal{O}(\Delta x + \Delta v) + \mathcal{O}(\varepsilon), \end{aligned}$$

which is consistent with the diffusion equation (2.5).

Using staggered grids  $x_{i+1/2}$  and a specific transport scheme for  $\rho$  enables us to obtain the standard centered scheme for the second derivative in (2.5):  $(\rho_{i+1} - 2\rho_i + \rho_{i-1})/\Delta x^2$ . These steps are fully detailed in [27].

For the mixed implicit version, when  $\varepsilon$  is small we get from (4.9)

$$h^n = \varepsilon T_{\varepsilon h_0}[\phi^n](\rho_i^n M_k) + \mathcal{O}(\varepsilon^2),$$

so that (4.7) becomes

$$\begin{aligned} \rho_i^{n+1} &= \rho_i^n - \beta \frac{\Delta t}{\varepsilon} \Pi(\mathcal{T}f)_{i,k}^n - (1 - \beta) \frac{\Delta t}{2\Delta x \varepsilon} \\ &\quad \times \Pi(v_k (h_{i+1,k}^{n+1} - h_{i-1,k}^{n+1})) + (1 - \beta) \frac{\Delta t^2}{\Delta t + \varepsilon^2} \\ &\quad \times \frac{\rho_{i+1}^{n+1} - 2\rho_i^{n+1} + \rho_{i-1}^{n+1}}{\Delta x^2}, \\ &= \rho_i^n - \beta \frac{\Delta t}{\varepsilon} \Pi(\mathcal{T}f)_{i,k}^n - (1 - \beta) \Delta t \partial_x (\rho^n \partial_x \phi^n)_i \\ &\quad + (1 - \beta) \frac{\Delta t^2}{\Delta t + \varepsilon^2} \partial_x^2 \rho_i^{n+1} + \mathcal{O}(\Delta x + \Delta v) + \mathcal{O}(\varepsilon), \end{aligned}$$

which is a consistent discrete scheme for the drift-diffusion equation with an implicit diffusion term.

## 5. Numerical results

We consider the following initial condition:

$$\begin{aligned} f(t=0, x, v) &= \frac{1}{a} \left( \exp \left( -\frac{1}{2\theta} |v - 2|^2 \right) \right. \\ &\quad \left. + \exp \left( -\frac{1}{2\theta} |v + 2|^2 \right) \right) (1 + \alpha \varphi(x)) \end{aligned} \quad (5.1)$$

where  $a$  is a normalization factor,  $\alpha = 10^{-3}$ ,  $\varphi(x) = \cos(kx + b_j)$ ,  $b_j$  being a random number between 0 and  $2\pi$ , and  $k$  is the wave number (here we use  $k = 0.2$ ). For the micro-macro model (2.8),

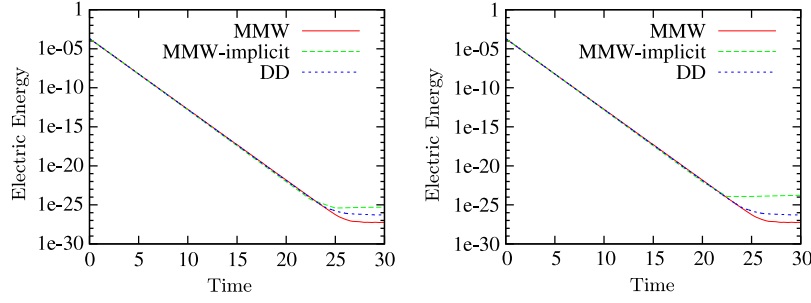


**Fig. 2.** Diffusive regime. Time history of the electric energy for  $\varepsilon = 10^{-4}$  (left) and  $\varepsilon = 10^{-8}$  (right) for the limit model (DD), the micro–macro model (MMW,  $\Delta t = 5 \times 10^{-3}$  for both values of  $\varepsilon$ ) and the micro–macro model with an implicit treatment of the diffusion (MMW-implicit,  $\Delta t = 5 \times 10^{-2}$  for both values of  $\varepsilon$ ).

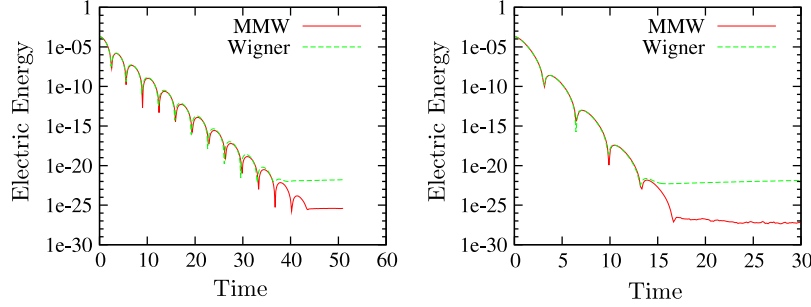


**Fig. 3.** Intermediate regime. Time history of the electric energy for  $\varepsilon = 1$  (left) and  $\varepsilon = 0.6$  (right).

the initial conditions read as

$$\rho(t=0, x) = 1 + \alpha\varphi(x), \quad \text{and}$$

$$g(t=0, x, v) = f(t=0, x, v) - \rho(t=0, x) \frac{\exp(-v^2/2)}{\sqrt{2\pi}}, \quad (5.2)$$

whereas for the limit model (2.5) we have

$$\rho(t=0, x) = 1 + \alpha\varphi(x).$$

The numerical parameters are chosen as follows:  $N_x = 300$ ,  $N_v = 512$  and  $\Delta t$  is chosen to respect the CFL condition  $\Delta t < \Delta x/v_{\max}$ , with  $v_{\max} = 20$ . As to the physical parameters, the normalized Planck constant is fixed to  $h_0 = 10^{-2}$ , the temperature is either  $\theta = 1$  or  $\theta = 0.2$ , and  $\varepsilon$  spans a wide range of values, from  $10^{-8}$  to  $10^4$ .

The cost of a numerical simulation using the MMW model is about twice the cost of a Wigner–BGK simulation in terms of computing time. Obviously, this cost is constant with respect to  $\varepsilon$ , whereas the cost of a Wigner simulation scales in  $1/\varepsilon^2$ .

We are interested in three regimes: the diffusive regime ( $\varepsilon \ll 1$ ), the intermediate regime [ $\varepsilon = \mathcal{O}(1)$ ], and the collisionless transport regime ( $\varepsilon \gg 1$ ). We shall compare the micro–macro Wigner–BGK model (2.8), here denoted by MMW, to either the drift-diffusion (DD) model (2.5) in the diffusive regime or to the full Wigner–BGK model (2.1) in the other regimes.

As a diagnostic tool, we consider the time history of the electric energy  $\|E(t)\|_{L^2}^2$  (the integral of the square of the electric field) for the three models, in the semi-log scale. In the collisionless regime, we also compare the numerical results to the analytical expression for the linear growth rate given in Section 3.

### 5.1. Diffusive regime

First, we consider very small values of  $\varepsilon$ . In Fig. 2, the electric energy is shown for the MMW (2.8) and DD (2.5) models, for  $\varepsilon = 10^{-4}$  and  $10^{-8}$ . For the two cases shown in Fig. 2, the time step for MMW is  $\Delta t = 5 \times 10^{-3}$ , which is much larger than the time step required for simulating the full Wigner equation

(2.1), which requires  $\Delta t = \mathcal{O}(\varepsilon^2)$ . Moreover, we also display the numerical results obtained by MMW with an implicit treatment of the diffusion (see the end of Section 4.1); for this scheme, we use a time step  $\Delta t = 5 \times 10^{-2}$ .

We notice that, for these values of  $\varepsilon$ , the diffusive regime is already attained, since the three curves (MMW and DD) are nearly superimposed. The observed damping of the electric energy is a consequence of the BGK relaxation operator, which acts to restore the equilibrium configuration  $M_\theta$ .

### 5.2. Intermediate regime

Here, we are interested in the intermediate regimes  $\varepsilon = \mathcal{O}(1)$ , for which the original Wigner–BGK model (2.1) can be simulated and compared to MMW. The time step  $\Delta t$  used for both MMW and Wigner–BGK is equal to  $10^{-3}$  (so that the CFL condition  $\Delta t < \Delta x/v_{\max}$  is satisfied).

The two models agree very well in this regime, as can be seen in Figs. 3 and 4. For the MMW model, the damping of the electric energy continues for longer times compared to the Wigner–BGK model. This behavior may be explained by the fact that the MMW code is less sensitive to round-off errors than the Wigner code.

We further consider the difference between  $f(x, v)$  (given by the Wigner scheme) and its micro–macro counterpart  $\rho(x)M(v) + g(x, v)$ , where  $M(v)$  is the absolute Maxwellian,  $\rho(x) = \int f(x, v)dv$ , and  $g(x, v)$  is the micro part of the distribution function. This quantity is plotted in Fig. 5 at a fixed velocity  $v = 0.5$  for  $\varepsilon = 1, 0.6$  and  $0.1$ , and in Fig. 6 at a fixed position  $x = 10$  for the same values of  $\varepsilon$ . Its maximum value is always very small ( $\approx 10^{-8} - 10^{-9}$ ) and is lower than  $\Delta t^2$ . Let us also recall that, for large values  $\varepsilon$ , this quantity vanishes by construction of the mixed scheme.

### 5.3. Collisionless transport regime

In this regime  $\varepsilon \gg 1$ . Thus, if we rescale the time  $t$  by  $t/\varepsilon$  in Eq. (2.1), we recover the standard collisionless Wigner–Poisson

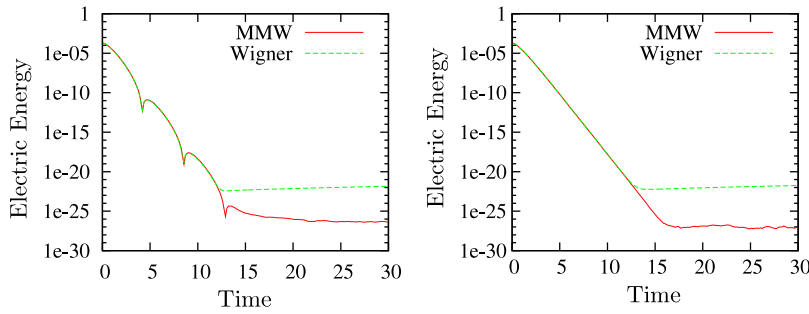


Fig. 4. Intermediate regime. Time history of the electric energy for  $\varepsilon = 0.55$  (left) and  $\varepsilon = 0.5$  (right).

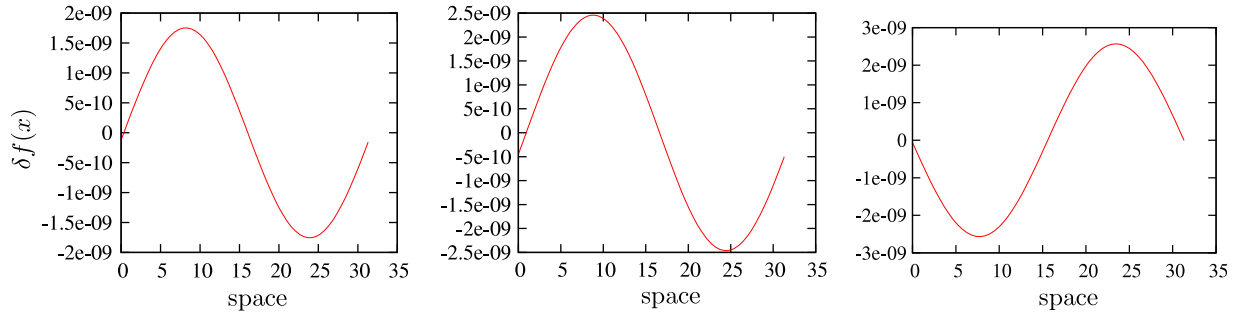


Fig. 5. Plot of  $\delta f(x) \equiv f(x, v = 0.5) - \rho(x)M(v = 0.5) - g(x, v = 0.5)$  as a function of  $x$ , at time  $t = 1$ , for  $\varepsilon = 1$  (left),  $\varepsilon = 0.6$  (middle), and  $\varepsilon = 0.1$  (right).

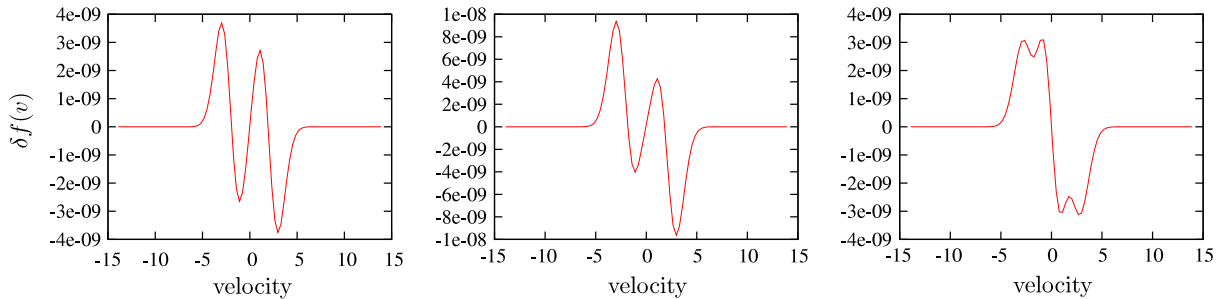


Fig. 6. Plot of  $\delta f(v) \equiv f(x = 10, v) - \rho(x = 10)M(v) - g(x = 10, v)$  as a function of  $v$ , at time  $t = 1$ , for  $\varepsilon = 1$  (left),  $\varepsilon = 0.6$  (middle), and  $\varepsilon = 0.1$  (right).

equations. We can therefore compare the numerical results to analytical estimates based on the linearization of the Wigner–Poisson equations (see Section 3).

In Fig. 7, we show the results for  $\varepsilon = 50$  and  $\varepsilon = 300$ . Again, the MMW and Wigner models yield practically the same results. The electric energy is still damped, but the damping rate is smaller compared to the diffusive and intermediate regimes. This is due to a competition between two effects: (i) on the one hand, the BGK term tends to damp the electric energy with a rate going as  $\varepsilon^{-1}$ ; (ii) on the other hand, the initial two-stream equilibrium is potentially unstable, which would lead to a growth of the electric energy. The net result is still damping, but with a lower rate.

Very large values of  $\varepsilon$  ( $10^3$  and  $10^4$ ) are considered in Figs. 8 and 9. Even in this regime, it is clear that the MMW code is capable of perfectly reproducing the Wigner–Poisson results. We note that, for  $\varepsilon = 10^3$ , the electric energy grows exponentially during the early stages of the simulation, signaling an instability (left panel of Figs. 8 and 9). The instability is even more visible in the zooms of these plots, shown in Fig. 10. Indeed, if we plug the relevant parameters ( $k = 0.2$ ,  $V = 2$ ,  $h_0 = 0.01$ ) in Eq. (3.9) for the linear frequency, we obtain  $\Omega^2 < 0$  so that the frequency has a non-zero imaginary part. For instance, for  $\varepsilon = 10^3$  and  $\theta = 0.2$ , one obtains  $\text{Im}(\Omega)/\varepsilon \approx 0.21$ , which is in good agreement with the observed

growth rate shown in the right panel of Fig. 10 (since the energy is a quadratic quantity in the electric field, the growth rate has to be multiplied by a factor two). For  $\theta = 0.2$  (left panel of Fig. 10) the agreement is also good.

Using the same parameters but taking  $\varepsilon = 10^4$  leads to a positive value of  $\Omega^2$  in Eq. (3.9), so that the frequency is a real quantity and no instability should occur. This is confirmed by the right panel of Figs. 8 and 9, where we see that the electric energy is damped away.

Finally, we note that this regime is well reproduced by the MMW code thanks to the use of the “mixed scheme” detailed in Section 4, which makes it possible to recover asymptotically an explicit numerical scheme for the Wigner–Poisson equations.

#### 5.4. Position-dependent $\varepsilon(x)$

In this paragraph, we consider the micro–macro Wigner–BGK model (2.8) in which the smallness parameter  $\varepsilon$  depends on the spatial variable  $x$  so that several regimes can coexist in the same simulation. The Wigner equation (2.1) should then be rewritten in the conservative form

$$\frac{\partial f}{\partial t} + v \partial_x \left( \frac{1}{\varepsilon(x)} f \right) - \frac{1}{\varepsilon(x)} T_{\varepsilon(x)h_0}[\phi] f = \frac{1}{\varepsilon^2(x)} (\rho M_\theta - f).$$



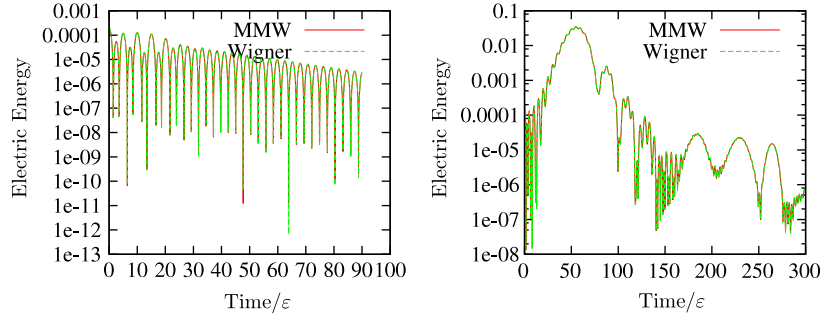


**Fig. 7.** Collisionless transport regime. Time history of the electric field for  $\varepsilon = 50$  (left frame) and  $\varepsilon = 300$  (right frame).

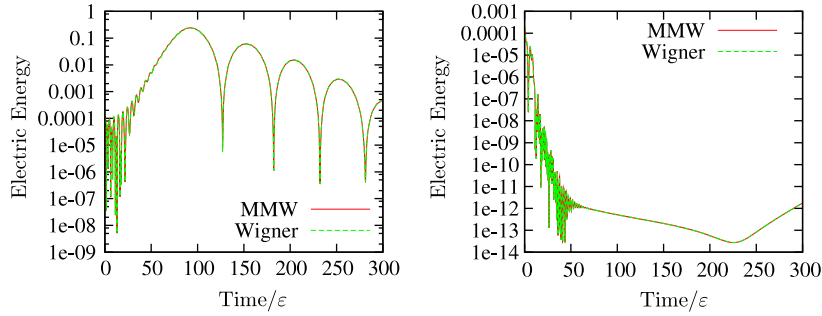


**Fig. 8.** Collisionless transport regime. Time history of the electric energy for  $\theta = 1$ ,  $\varepsilon = 10^3$  (left frame) and  $\varepsilon = 10^4$  (right frame).

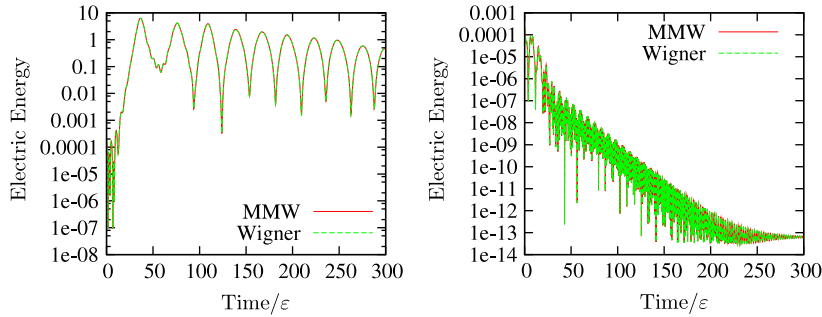


**Fig. 9.** Collisionless transport regime. Time history of the electric energy for  $\theta = 0.2$ ,  $\varepsilon = 10^3$  (left frame) and  $\varepsilon = 10^4$  (right frame).

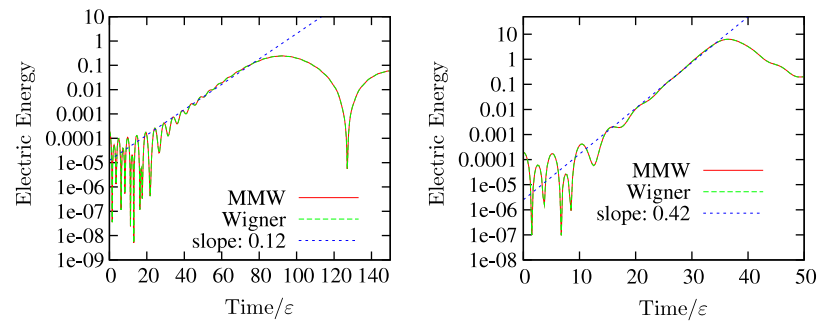


**Fig. 10.** Zoom of the left frames in Figs. 8 and 9.  $\varepsilon = 10^3$  and  $\theta = 1$  (left frame);  $\varepsilon = 10^3$  and  $\theta = 0.2$  (right frame). The slope of the dashed straight lines corresponds to the instability rate multiplied by two.

This type of problem has already been investigated in the hydrodynamic regime [28]. A similar profile for  $\varepsilon(x)$  is considered here

$$\varepsilon(x) = \varepsilon_0 + \varepsilon_{\max} \exp\left(-\frac{|x - \pi/k|^2}{4}\right), \quad x \in [0, 2\pi/k],$$

where  $k = 0.2$ ,  $\varepsilon_0$  is a threshold value for  $\varepsilon(x)$ , and  $\varepsilon_{\max}$  can in principle be very large. This spatial profile of  $\varepsilon(x)$  represents a

system where a collisionless region is surrounded by two strongly collisional buffer zones.

The micro-macro model is well suited for this kind of situation, since the time step  $\Delta t$  is chosen to respect the CFL condition  $\Delta t < \Delta x/v_{\max}$ , whereas for the full Wigner model one needs to take  $\Delta t < \varepsilon_0^2$ , which can be too restrictive when  $\varepsilon_0$  is small.

Two cases will be considered here. First, we set  $\varepsilon_0 = 0.1$  and  $\varepsilon_{\max} = 10$  so that comparisons between the MMW and

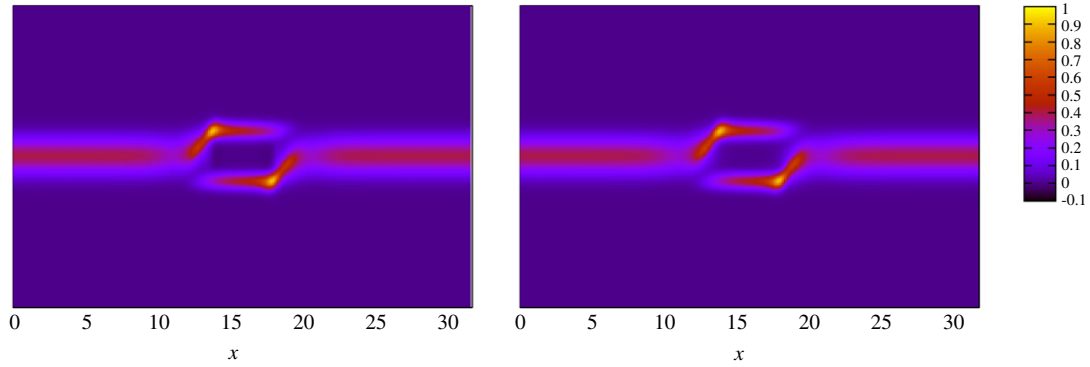


**Fig. 11.** Phase space distribution function  $f(x, v)$  at time  $t = 0.1$ . Left frame: MMW; right frame: Wigner.

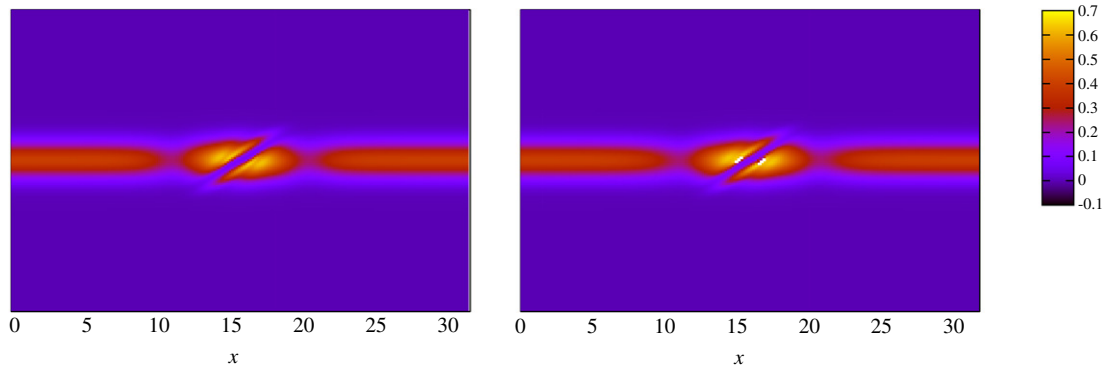


**Fig. 12.** Phase space distribution function  $f(x, v)$  at time  $t = 2$ . Left frame: MMW; right frame: Wigner.

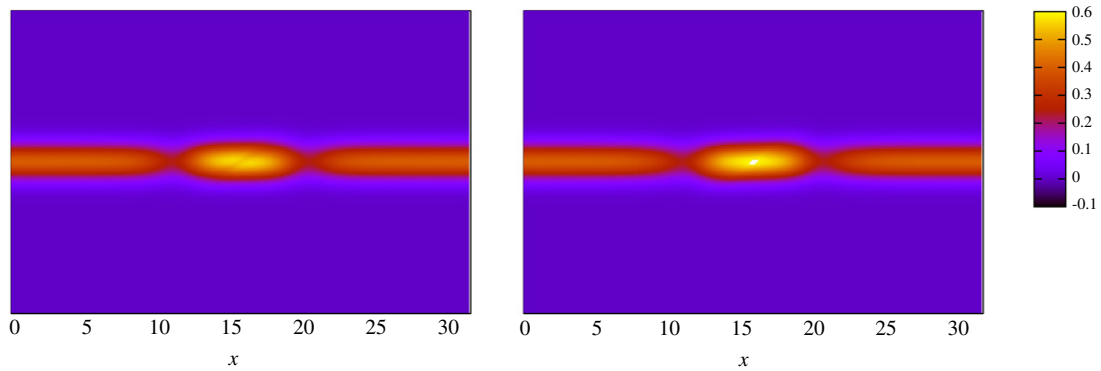


**Fig. 13.** Phase space distribution function  $f(x, v)$  at time  $t = 10$ . Left frame: MMW; right frame: Wigner.

Wigner models can still be performed (we use  $\Delta t = 10^{-3}$  for both schemes). In the second case, we shall take  $\varepsilon_0 = 10^{-7}$  and  $\varepsilon_{\max} = 10^3$ . For this value of  $\varepsilon_0$ , Wigner simulations are not feasible and therefore only the MMW results will be shown, which are obtained with a time step  $\Delta t = 5 \times 10^{-4}$ .

We use the same initial condition (5.1)–(5.2) as in the cases with constant  $\varepsilon$  and the number of points in the phase space is  $N_x = 200, N_v = 256$ . We are interested in the density  $\rho(x)$  as well as the full distribution function  $f(x, v)$  at different times (for the MMW scheme, the distribution function is  $f_{\text{MMW}} = \rho(x) \exp(-v^2/2)/\sqrt{2\pi} + g(x, v)$ ).

In Figs. 11–13, we plot the phase-space distribution function at times  $t = 0.1, 2$  and  $10$ , obtained with the Wigner and MMW schemes, for the case  $\varepsilon_0 = 0.1$  and  $\varepsilon_{\max} = 10$ . For early times, a vortex is created in the middle of the domain, where the plasma is essentially collisionless. Outside this domain the plasma quickly becomes strongly collisional so that the formation of phase space structures is inhibited. The transition to the diffusive regime

occurs around  $x = 10$  and  $x = 20$ . Even in the middle of the domain, the collisions bring the system back to equilibrium for later times ( $t = 20$ ).

We stress that the phase space plots obtained from the Wigner and MMW models are virtually identical. The good behavior of the MMW scheme is emphasized in Fig. 14, where the densities  $\rho(x)$  obtained with the two methods are displayed at  $t = 1$ .

For the second run, we take  $\varepsilon_0 = 10^{-7}$  and  $\varepsilon_{\max} = 10^3$ . In this case, the Wigner scheme cannot be used as it would require a time step  $\Delta t \sim \varepsilon_0^2$ . Hence, only numerical results obtained with the MMW method are shown. In Fig. 15, the distribution function  $f(x, v)$  is plotted at time  $t = 1$ , whereas the spatial density  $\rho(x)$  is displayed in Fig. 16. As in the previous case, a transition zone – separating the diffusion regime from the collisionless regime – can be clearly identified around  $x = 10$  and  $x = 20$ .

Note that this case is rather challenging, since the numerical scheme must be capable of handling two very disparate regimes at the same time. An alternative strategy – in which a diffusion model

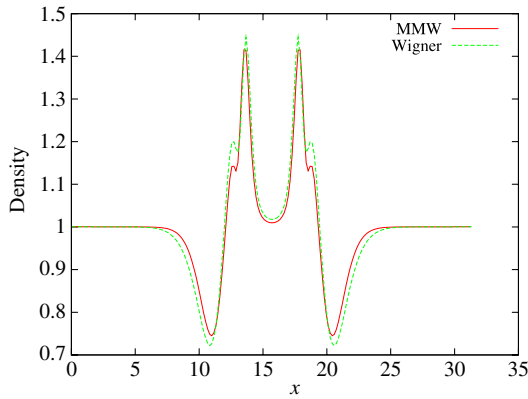


**Fig. 14.** Spatial density  $\rho(x)$  at time  $t = 1$  obtained with the MMW scheme (solid red line) and the Wigner scheme (dashed green line). (For interpretation of the references to colour in this figure legend, the reader is referred to the web version of this article.)

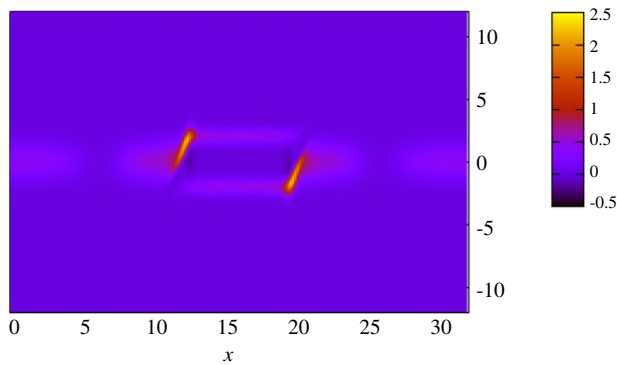


**Fig. 15.** Distribution function at time  $t = 1$  obtained with the MMW scheme:  $f_{\text{MMW}}(t = 1, x, v) = \rho(t = 1, x) \exp(-v^2/2)/\sqrt{2\pi} + g(t = 1, x, v)$ .

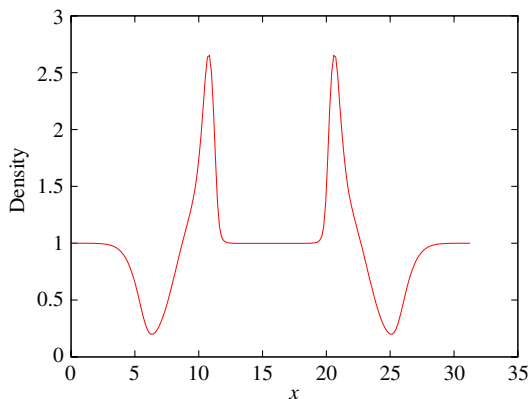


**Fig. 16.** Spatial density  $\rho(x)$  at time  $t = 1$  obtained with the MMW scheme.

such as Eq. (2.5) is used in the small  $\varepsilon$  region and a Wigner model is used in the large  $\varepsilon$  region – would require some carefully tailored boundary conditions at the interface between the two subdomains, which is usually a very delicate task.

## 6. Conclusion

In this work, we developed a micro–macro numerical scheme for the Wigner–Poisson–BGK equation (named the MMW scheme),

which satisfies the following asymptotic properties: (i) when  $\varepsilon \rightarrow 0$ , it reduces to a consistent discretization of the drift–diffusion equation, for a fixed set of numerical parameters that is not restricted by  $\varepsilon$ ; (ii) when  $\varepsilon \rightarrow +\infty$ , it reduces to the original explicit discretization of the collisionless Wigner–Poisson equation.

Numerical tests have proven that the MMW scheme reproduces correctly the results of the drift–diffusion model in the limit  $\varepsilon \rightarrow 0$  and those of the Wigner–Poisson model when  $\varepsilon = O(1)$  or  $\varepsilon \gg 1$ . In addition, when  $\varepsilon$  is very large, the numerical computations agree with the analytical calculations of the linear instability rates.

Finally, we studied the case of a spatially dependent  $\varepsilon$ , for which this approach is well suited, since no domain decomposition is required and the AP scheme can be applied to the whole domain using a fixed set of numerical parameters. Again, the comparison between the MMW and Wigner schemes yielded very satisfactory results.

Several extensions of the present work may be envisaged. More physically realistic collision operators (e.g., Fokker–Planck) could be considered and the present strategy could be extended along the ideas presented in [32]. It would also be interesting to use higher order numerical schemes for the phase space discretization of the micro–macro model.

## References

- [1] E.P. Wigner, *Phys. Rev.* 40 (1932) 749.
- [2] M. Hillery, R.F. O’Connell, M.O. Scully, E.P. Wigner, *Phys. Rep.* 106 (1984) 121.
- [3] N.C. Kluksdahl, A.M. Kriman, D.K. Ferry, C. Ringhofer, *Phys. Rev. B* 39 (1989) 7720.
- [4] P.A. Markowich, C.A. Ringhofer, C. Schmeiser, *Semiconductor Equations*, Springer, Vienna, 1990.
- [5] R. Jasiak, G. Manfredi, P.-A. Hervieux, M. Haefele, *New J. Phys.* 11 (2009) 063042.
- [6] G. Manfredi, P.-A. Hervieux, *Appl. Phys. Lett.* 91 (2007) 061108.
- [7] A. Arnold, C. Ringhofer, in: K. Hess (Ed.), *Semiconductor Transport and Device Simulation*, 1992, p. 198.
- [8] T. Goudon, *SIAM J. Numer. Anal.* 40 (2002) 2007.
- [9] C. Ringhofer, *Math. Models Methods Appl. Sci.* 2 (1991) 91.
- [10] C. Ringhofer, *Acta Numer.* 3 (1997) 485.
- [11] S. Jin, *SIAM J. Sci. Comput.* 21 (1999) 441.
- [12] N. Ben Abdallah, P. Degond, *J. Math. Phys.* 37 (1996) 3306.
- [13] L. Barletti, G. Frosali, *J. Stat. Phys.* 139 (2010) 280.
- [14] F. Méhats, L. Barletti, *J. Math. Phys.* 51 (2010) 053304.
- [15] A. Jüngel, *Transport Equations for Semiconductors*, Springer, Berlin, 2009.
- [16] A. Jüngel, *Quasi-Hydrodynamic Semiconductor Equations*, Birkhäuser, Basel, 2001.
- [17] P. Degond, F. Méhats, C. Ringhofer, *J. Stat. Phys.* 118 (2005) 625.
- [18] S. Jin, D. Levermore, *Transport Theory Statist. Phys.* 22 (1993) 739.
- [19] C. Ringhofer, *SIAM J. Numer. Anal.* 38 (2000) 442.
- [20] J.A. Carrillo, T. Goudon, P. Lafitte, F. Vecil, *J. Sci. Comput.* 36 (2008) 113.
- [21] A. Klar, *SIAM J. Numer. Anal.* 19 (1998) 2032.
- [22] A. Klar, *SIAM J. Numer. Anal.* 35 (1998) 1073.
- [23] A. Klar, *SIAM J. Sci. Comput.* 20 (1999) 1696.
- [24] A. Klar, C. Schmeiser, *Math. Models Methods Appl. Sci.* 11 (2001) 749.
- [25] S. Jin, D. Levermore, *J. Comput. Phys.* 126 (1996) 449.
- [26] S. Jin, L. Pareschi, G. Toscani, *SIAM J. Numer. Anal.* 38 (2000) 913.
- [27] M. Bennoune, M. Lemou, L. Mieussens, *J. Comput. Phys.* 227 (2008) 3781.
- [28] F. Filbet, S. Jin, *J. Comput. Phys.* 229 (2010) 7625.
- [29] N. Crouseilles, M. Lemou, *Kinet. Relat. Models* 4 (2011) 441.
- [30] S. Jin, L. Wang, *Acta Math. Sci.* 31 (2011) 2219.
- [31] M. Lemou, L. Mieussens, *SIAM J. Sci. Comput.* 31 (2008) 334.
- [32] M. Lemou, *C. R. Math.* 348 (2010) 455.
- [33] C. Ringhofer, *Transport Theory Statist. Phys.* 31 (2002) 431.
- [34] A. Arnold, J.-A. Carrillo, I. Gamba, C.-W. Shu, *Transport Theory Statist. Phys.* 30 (2001) 121.
- [35] M. Lemou, L. Méhats, *SIAM J. Sci. Comput.* 34 (2012) 734.
- [36] N.W. Ashcroft, N.D. Mermin, *Solid State Physics*, Harcourt Brace, Orlando, 1976.
- [37] I.M. Gamba, M.P. Gualdani, C. Sparber, *Kinet. Relat. Models* 2 (2009) 181.
- [38] J.-G. Liu, L. Mieussens, *SIAM J. Numer. Anal.* 48 (2010) 1474.
- [39] N.-D. Suh, M.R. Feix, P. Bertrand, *J. Comput. Phys.* 94 (1991) 403.